ELSEVIER

European Journal of Cancer 41 (2005) 1875–1888

European Journal of Cancer

www.ejconline.com

Karyometry in the early detection and chemoprevention of intraepithelial lesions

J. Ranger-Moore [a,*], D.S. Alberts [a], R. Montironi [b], F. Garcia [a], J. Davis [a], D. Frank [a], M. Brewer [a], G.M. Mariuzzi [c], H.G. Bartels [a], P.H. Bartels [a]

[a] *University of Arizona, P.O. Box 245024, Tucson, Arizona, AZ 85724-5024, USA*
[b] *Polytechnic University of the Marche Region ef, Ancona, Italy*
[c] *University of Verona, Verona, Italy*

Received 4 May 2005; received in revised form 1 July 2005; accepted 6 July 2005
Available online 8 August 2005

Abstract

The ideal chemopreventive agent targets pre-neoplastic changes and intraepithelial neoplasia, preventing progression over time without notable side effects. Assessment of success of chemopreventive intervention in the short and medium term remains a challenge, and in this review the suggestion is investigated that karyometric measurements constitute suitable markers of chemopreventive efficacy. Karyometry provides the sensitivity required to detect small differences amidst relatively high biological variability. It can help establish progression curves of intraepithelial neoplasia (IEN) to invasive cancer, and thus detect chemopreventive effects. Such effects can be observed in two ways, at the group level (intervention vs. placebo), and at the case (or patient) level. The latter is more difficult to establish, necessitating the development of specialised statistical methods. Analysis of between-case and within-case heterogeneity can reveal useful information about cancer progression and prevention. We suggest that karyometry can objectively quantify IEN progression, providing a framework for statistically securing chemopreventive effects. It can act as an integrating biomarker by detecting chemopreventive activity even when the mechanism for a given progression pathway is unknown, or when multiple pathways exist. The sensitivity of karyometric detection can help optimise the design of clinical trials of novel chemopreventive agents by decreasing trial duration and/or sample size.

Keywords: Chemoprevention; Intraepithelial lesions; Pre-neoplastic lesions; Karyometry; Progression curves; Measurement of efficacy

1. Introduction

The ideal chemopreventive agent would halt the progression of existing intraepithelial lesions, reverse any neoplastic or pre-neoplastic conditions and changes, and otherwise reliably prevent the development of any such lesions in the first place. The agent should accomplish this without significant side effects, so that those who do not have overt disease can take it over long periods of time. The need for subtle, gentle intervention suggests that the most promising targets of chemopreventive intervention are likely to be precursor lesions, such as intraepithelial neoplasia (IENs).

The gold standard for detecting change in intraepithelial neoplastic tissue remains expert histopathologic assessment. However, such assessment is extremely difficult for very early stages of deviation from normal, as seen in pre-neoplastic lesions. The term pre-neoplasia is used in this paper to denote lesions in tissue section regions that are visually diagnostically assessed as normal, *i.e.*, the very early changes that commence the progression pathway to cancer, but have not yet become visibly apparent. Pre-neoplastic change is documented by computer analysis in comparison to histologically

* Correspondence author. Tel.: +1 520 626 3118; fax: +1 520 626 2467.
E-mail address: jrangerm@azcc.arizona.edu (J. Ranger-Moore).

0959-8049/$ - see front matter © 2005 Elsevier Ltd. All rights reserved.
doi:10.1016/j.ejca.2005.07.002

normal lesions from organs not harboring a pre-malignant or malignant lesion. Once a lesion has become visually apparent, we refer to it as pre-malignant or malignant. Pre-neoplastic lesions, as defined here, have been karyometrically documented in histologically normal appearing tissue of organs harboring premalignant or malignant lesions and even in histologically normal appearing tissue of patients at high risk for the development of such lesions. Pre-neoplastic lesions exhibit – in attenuated form – the characteristic karyometric signatures of premalignant and malignant lesions. One would logically expect chemopreventive intervention to be most effective in halting and even reversing the earliest expression of deviation from normal. Pre-neoplastic lesions may therefore become one of the most important targets for testing chemopreventive agents for efficacy.

The nuclear chromatin pattern has for a long time provided important diagnostic clues. The changes in its spatial and statistical distribution were systematically related to neoplastic progression in seminal studies by Grundmann [1]. The increase in "heterochromatisation" associated with progression to malignancy was the subject of numerous studies in the 1950s, *e.g.* the studies by Harbers and Sandritter [2]. It is true that the nuclear chromatin pattern is influenced by the fixation process, but the resulting pattern observed has been demonstrated to be highly reproducible and very specific for the functional state of a nucleus. The quantification of the spatial distribution of the nuclear chromatin pattern has allowed the detection of very subtle changes, due to the considerable analytic power of multivariate statistical procedures and computer assisted data mining. Pre-neoplastic lesions have been documented in numerous organ sites, including prostate [3], breast [4–6], ovary [7,8], cervix [9–17], lung [18], colon [19,20], esophagus [21], thyroid [22,23] and bladder [24].

Karyometry offers many characteristics desirable for measuring chemopreventive efficacy. The nuclear chromatin pattern responds in a highly sensitive manner to any change in the metabolic state of a nucleus. It responds quickly to such changes and is able to reflect reversible events. The pronounced changes in the nuclear chromatin distribution seen in the progression of prostatic intraepithelial lesions (PIN) constitutes a good example [3,25]. It has also been shown by microarray technology that when cells from these high grade lesions are brought into interaction with laminin-5 an upregulation of numerous genes can be observed within hours [26]. It is appropriate to remember here, that the chromatin pattern reflects not only DNA distribution within the nucleus, but even more importantly enveloping histones, where genes are regulated. The hematoxylin staining records these changes.

The need to detect subtle effects in a background of biological variability inherent in samples obtained in real-world clinical trials poses a significant challenge in this field of research. This article presents some of the problems encountered in measuring chemopreventive efficacy, and methodology that has been developed to address those problems. Initially, we present an overview over technical and statistical methods. Then, we survey results that illustrate the ability of karyometry to: (1) establish progression curves, which are useful yardsticks to measure change as a result of chemopreventive intervention; (2) exhibit great sensitivity of detection; (3) accommodate between- and within-case heterogeneity; (4) detect pre-neoplastic lesions in samples from organ sites with or without co-occurring premalignant or malignant lesions; and (5) utilise recently developed second-order analytical methods to detect small differences. All of these characteristics are important elements to aid the search for effective chemopreventive agents. In many cases presented here, karyometric results are linked to histopathologic findings. However, they are also linked to progression curves that contain advanced diagnostic categories, such as advanced hyperplasia and carcinoma, which have strong clinical relevance. Finally, in some cases, we correlate karyometric findings with clinical outcomes directly.

2. Materials and methods

Because karyometry as applied to chemoprevention seeks to detect subtle differences in the midst of considerable biological heterogeneity, the importance of avoiding extraneous sources of bias or variability cannot be overemphasised. Fixation and staining of materials must be strictly controlled. We have found it useful to incorporate and monitor control slides using material from human tonsil or skin to maintain quality control in the staining process. Also, imaging and segmentation must be conducted by trained personnel whose performance is monitored over time. As much as possible, material for a given study should be stained in a minimal number of batches, and image processing should ideally be performed by a single, trained individual.

For histologic specimens, clinical materials are fixed in 10% neutral buffered formalin, paraffin- embedded, cut to 5 μm sections and stained under carefully controlled conditions by a routine hematoxylin–eosin procedure. For cytologic preparations, alcohol fixation and pap staining are typically performed. Other routine approaches can also be utilised, provided that consistency of preparation is maintained within any given study. Areas to be sampled are visually assessed and selected by expert pathologists. Within such regions, nuclei are imaged, and a random sample of non-overlapping, well-focused nuclei is selected for imaging. Imagery of prepared slides is recorded on a videomicrophotometer equipped with a 63:1 planapochromatic oil

immersion objective of 1.4 N.A. Relay optics adjust the sampling to 6 pixels per linear micron. Meticulous photometric calibration, linearity correction and uniformity of background correction are maintained.

Images of nuclei are segmented by a semiautomated procedure, with manual correction. The extraction of karyometric features provides approximately 100 features descriptive of the spatial and statistical distribution pattern of the nuclear chromatin. A standardised deviation of each feature from a reference value recorded from a sample of normal reference nuclei is computed. The average of these deviations formed over all karyometric features is computed as the ''nuclear abnormality'' [27]. This measure, including all karyometric information, is robust. Discriminant function scores are more specifically targeted and thus more sensitive. Two kinds of discriminant functions are used. The first is based on a regular stepwise discriminant function algorithm and derived as a linear combination of a small selected subset of karyometric features. The subset is obtained by means of a non-parametric test comparing all features between two or more data sets of interest. The other, referred to as a ''second order'' discriminant function [28], is based on meta-features derived from the distribution pattern of features or first order discriminant function scores as found in every case.

Due to the structure of the data (nuclei nested within biopsies, which if multiple biopsies per person are taken, are also nested within person), valid *P*-values can be obtained through the use of mixed models that account for nesting effects. The utility of this approach has been noted in the literature [29–31], but its application is as yet far from universal. A mixed model approach is a suitable parametric model for the analysis of continuous outcomes, such as nuclear abnormality, or categorical outcomes, such as case classification. However, other approaches, some parametric and some non-parametric, may also be employed. A number of these have been usefully assessed by Wolfe and her colleagues [32]. It is of interest to note that some of these approaches also appear in the analysis of microarray data, another arena where the number of features (genes, in microarray analysis) typically outweighs the number of cases. However, the development of new feature spaces, as with the development of second order discriminant functions, suggests that perhaps the difference in feature space size may be limited only by the creativity of the data analyst. Certainly, the most successful analyses will involve a combination of data mining techniques and confirmatory statistical validation. The more extensive the data mining, the greater the need for validation.

While mixed models account for within biopsy correlation structures, little attention has been paid to within-subject between-biopsy heterogeneity. Simply put, if one takes a single biopsy from an individual, how representative is it of all possible biopsies? Currently, we are studying triplicate biopsies in rectal mucosa and in sun-damaged skin to assess the degree of heterogeneity present. The results will inform study design, answering the question of how to balance the number of study subjects with the number of biopsies per subject that should be taken to maximise statistical power. Sample size methods that were originally developed for group-randomised trials can be usefully applied once knowledge of within-biopsy and within-subject between-biopsy heterogeneity has been gained [33,34].

3. Results

3.1. Progression curves

Most measures of deviation from normal show a monotonic trend in values from those observed in nuclei from normal tissues to values found in nuclei from low-grade and high-grade premalignant lesions. They thus lend themselves to construction of a progression curve. The progression curve is a useful analytic tool to follow and assess changes in lesion development from initiation and promotion to progression or reversal due to chemopreventive intervention. The progression curve is not meant to represent a biologic event, although it is possible that actual lesion development may follow such a trend.

A typical progression curve is shown for prostate lesions in Fig. 1. Here, a discriminant score was chosen as the ordinate. Note the data points for the diagnostic categories: norm/low grade PIN, norm/high grade PIN and norm/cancer. They represent nuclei measured in histologically normal appearing tissue of prostates harboring

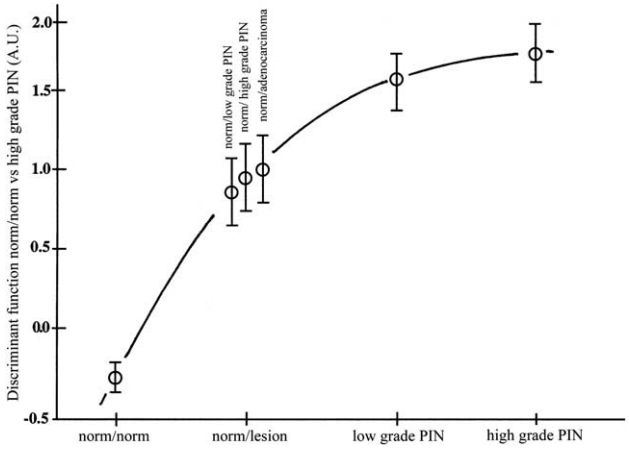

Fig. 1. Progression curve for prostatic intraepithelial neoplastic lesions. Norm/norm identifies nuclei from normal prostatic tissue from lesion-free prostates. Norm/lesion identifies nuclei from histologically normal-appearing tissue of prostates harboring a particular lesion. Note how the preneoplastic lesions fall between normal and low-grade PIN. Data derived from [3].

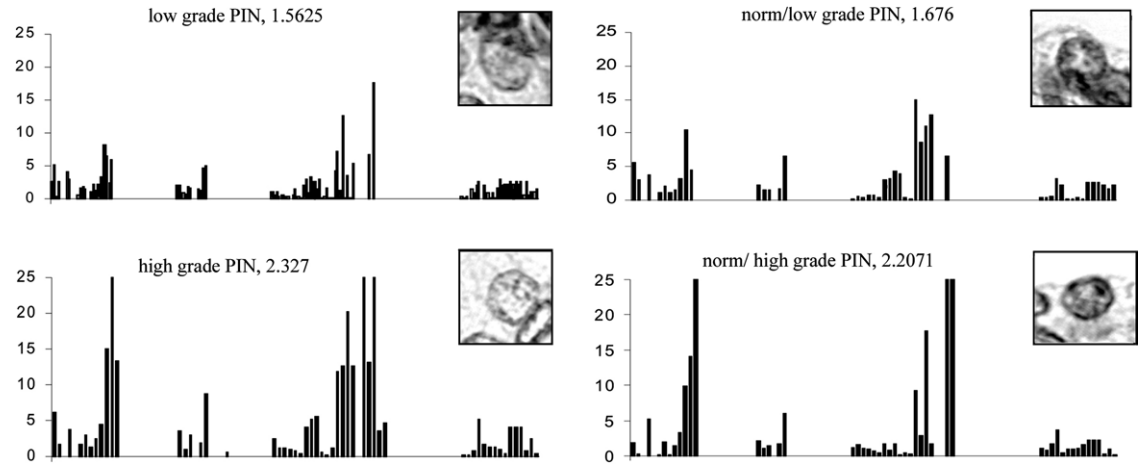

Fig. 2. Nuclear signatures of nuclei from low grade and high grade PIN at left, and from normal appearing tissue of prostates harboring low or high-grade PIN lesion at right. Note the similarity of signatures seen in the pre-neoplastic and IEN lesions. Data derived from [27].

a premalignant or malignant lesion, *i.e.*, they are from a pre-neoplastic lesion.

Nuclei in pre-neoplastic lesions show a nuclear signature similar to that of the premalignant or malignant lesion in the organ, but in an attenuated form. This is shown for the nuclei measured in the histologically normal appearing tissue of prostates harboring a low grade or high grade PIN lesion in Fig. 2. Fig. 3 shows a progression curve for colonic lesions (numeric data not shown). Again, the normal appearing mucosa in cases harboring adenoma or an adenocarcinoma deviates from normal, as a pre-neoplastic change. A progression curve for endometrial lesions is plotted in Fig. 4 [35]. The average nuclear abnormality value is used as ordinate, and a discriminant function score as abscissa.

One may relate a measure for progression of a lesion to relative risk for the development of invasive disease. This is shown in Fig. 5 for ductal carcinoma *in situ* (DCIS) lesions of the breast [36,37]. A location on the abscissa, such as the diagnostic label "DCIS solid", should not be interpreted as a sharply defined location: it represents a fuzzy membership function and a value observed for a given case should actually be projected sideways onto the progression curve. It is noteworthy that the curve exhibits a monotonic trend, suggesting a continuous progression, whereas the actual lesions exhibit very different histologic architec-

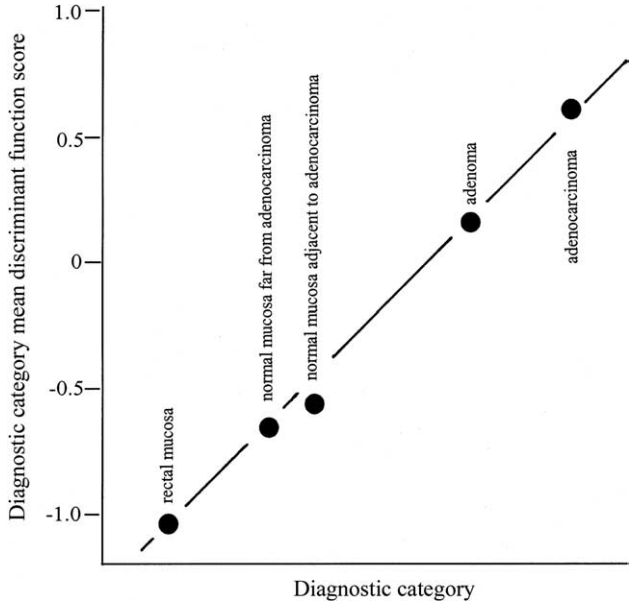

Fig. 3. Progression curve for colonic lesions. Note the position of the nuclei recorded in the histologically normal appearing mucosa distant and adjacent to adenocarcinoma, indicating a pre-neoplastic lesion.

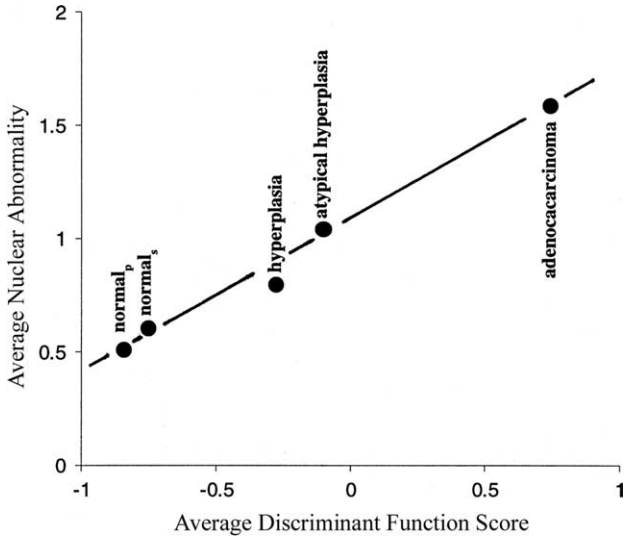

Fig. 4. Progression curve for endometrial lesions. Measurements in normal tissue were taken in the proliferative and in the secretory phase. Data derived from [35].

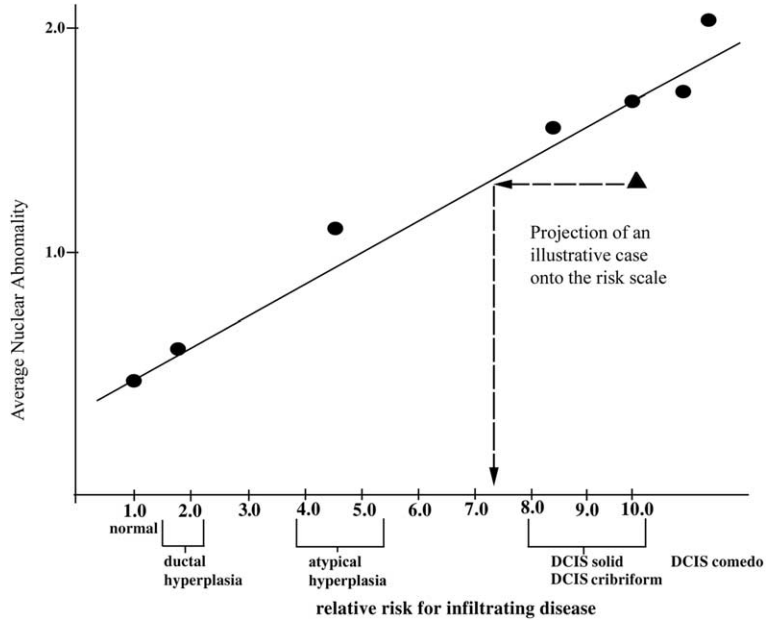

Fig. 5. Progression curves for premalignant breast lesions. Average nuclear abnormalities are plotted against relative risk ranges for invasive disease. Data derived from [36].

tures that do not necessarily evolve from one to the other.

The true progression of a lesion is assessed more accurately if nuclei not actually deviating from normal – but recorded due to the protocol demanding random sampling in a circumscribed area – are thresholded out, as shown in Fig. 6, for nuclei from Barrett's esophagus. In the absence of such thresholding, the resulting within-case nuclear heterogeneity attenuates the ability to assess change and differences. This will be explored more fully below. Upon thresholding, one obtains a corrected progression curve, as seen in Fig. 7 [21].

To describe the progression of a pre-neoplastic or premalignant lesion, one may use the proportion of nuclei for which a discriminant function score exceeds a certain threshold. In spirit, this parallels the earlier described technique of choosing only nuclei for analysis beyond a certain threshold, but this approach possesses distinct statistical properties. Fig. 8 shows such an example for colonic tissue. Note that the proportion of nuclei sampled in the histologically normal appearing tissue, adjacent to adenocarcinoma and the proportion distant from such a lesion are approximately the same in this data set.

The use of a progression curve to assess chemopreventive efficacy of 2-(difluoromethyl)-DL-ornithine (DFMO) in solar keratotic lesions proved useful [38]. Fig. 9 shows a previously established progression curve based on the 10% worst nuclei on the basis of average nuclear abnormality, with a discriminant function value

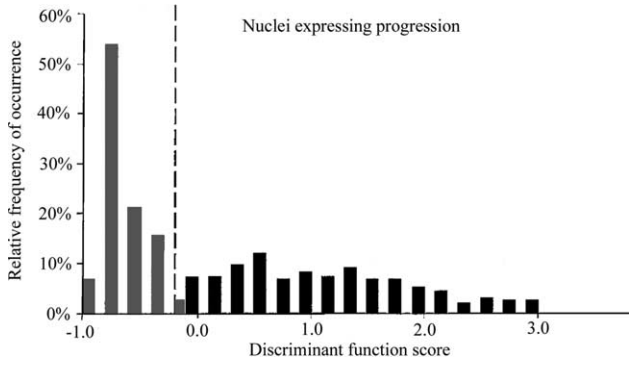

Fig. 6. Distribution of discriminant function scores for nuclei from Barrett's esophagus. The threshold is set to exclude normal nuclei from an assessment of the degree of lesion progression. Data derived from [21].

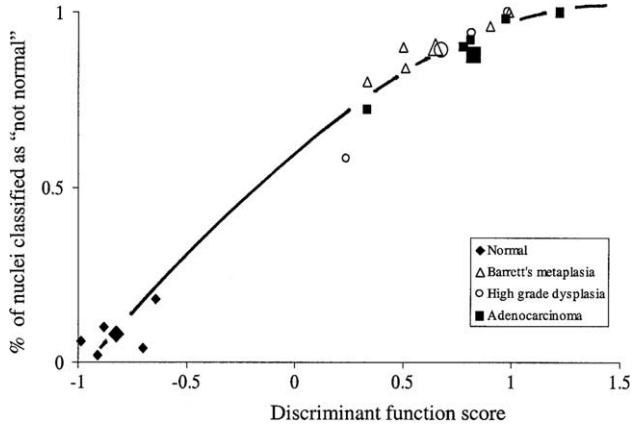

Fig. 7. Proportion of nuclei from classified as "not normal" plotted over the average discriminant function score per case, showing considerable overlap of Barrett's metaplasia with the other diagnostic categories. Group means are indicated by the enlarged symbols. Data derived from [21].

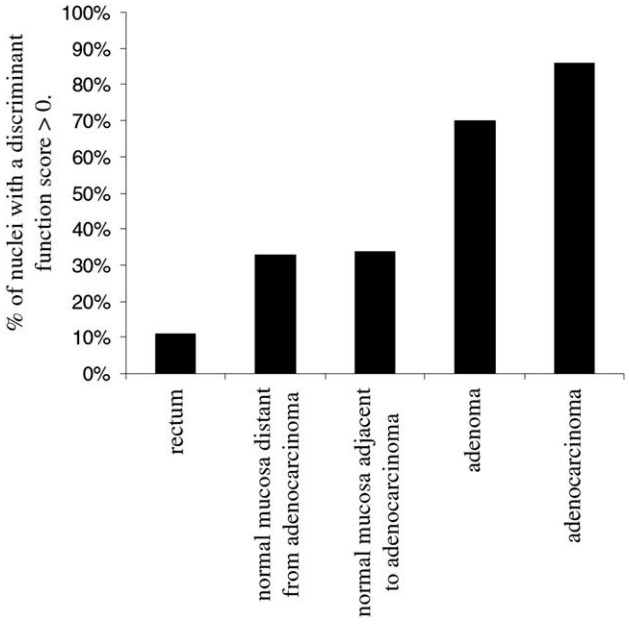

Fig. 8. Proportion of nuclei deviating from normal in colonic lesions.

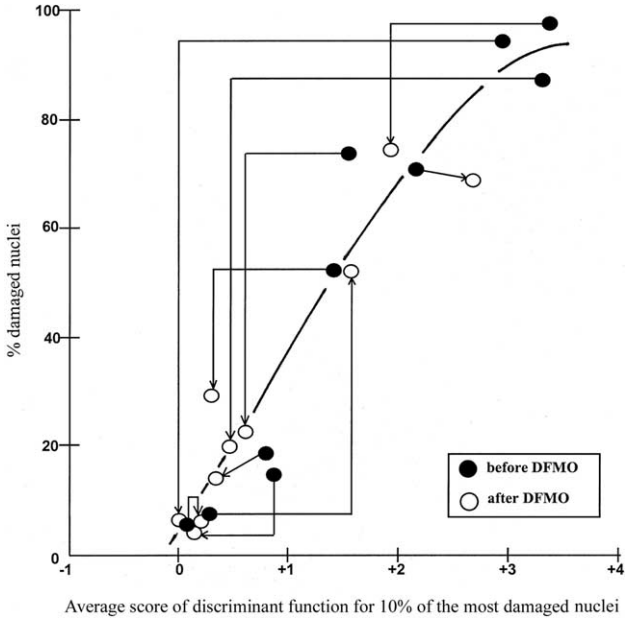

Fig. 9. Measurement of chemopreventive efficacy of DFMO in skin lesions, Data derived from a pilot study [38].

as abscissa, and the proportion of nuclei with actinic damage as ordinate. Taking the 10% worst nuclei is equivalent to establishing thresholds that are case-specific. The graph shows the change in the proportion of damaged nuclei for each case at baseline and at end of study. In this data set from a feasibility study, 8/10 cases showed a reduction in the proportion of damaged nuclei. This finding correlates directly with the clinical findings, *i.e.*, that DMFO also resulted in a statistically significant reduction in the number of actinic keratoses.

3.2. Sensitivity of karyometric methodology

The distribution of nuclear abnormality values, also called the "lesion signature", is an eminently useful representation. It does not respond as sensitively as a distribution of discriminant function scores, but nuclear abnormality has proven itself as a robust and reliable measure. Fig. 10 shows the lesion signatures for a placebo treatment group before and after intervention in a study of solar actinic damage [39,40]. The bulk of nuclei show abnormality values in the 0.4–0.7 range, as expected for normal, undamaged nuclei. But, in both the baseline and the end of study data sets a proportion of nuclei show abnormality values averaged over about 100 karyometric features deviating up to 1.5 standard deviations from normal reference tissue.

If one records the pattern of change in the intervals of such a distribution two valuable statistics are obtained. One can obtain both an estimate of the net proportion of nuclei undergoing a change and an estimate of the significance of the pattern of change, *e.g.*, by a runs test [41]. In the example of Fig. 10, a net total of 13.7% of nuclei incur increased actinic damage during the trial period. In this instance the systematic shift towards increased abnormality was particularly clear-cut. One can use a minus sign (−) for histogram bins where the

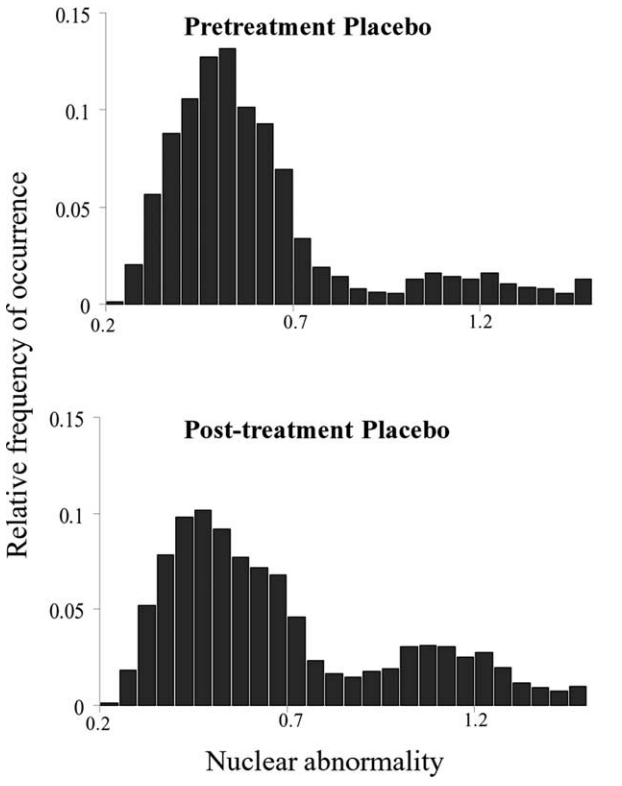

Fig. 10. Distributions of nuclear abnormality in sun-exposed skin in biopsies taken one year apart. Data derived from the placebo arm of a recent chemoprevention efficacy study [40].

proportion of nuclei decreases, and a plus sign (+) for histogram bins where it increases. Starting from the lowest interval of nuclear abnormality the relative frequencies of occurrence of nuclei decrease for the first ten bins, and increase in the following fourteen bins towards higher abnormality values, resulting in the following pattern: ----------++++++++++++++. There are only two runs, clearly not a random sequence, but rather a highly statistically significant shift ($p < 0.001$).

3.3. Between case heterogeneity

Between-case heterogeneity can readily become a limiting factor in the detection of efficacy, but it can also reveal prognostically important information. In a clinical trial, biopsies from 129 cases of rectal mucosa were collected from patients with a prior history of colonic adenoma [20]. Among these cases were 57 who experienced recurrent disease and 72 cases without recurrence on follow-up colonoscopy (follow-up time was 3–5 years). All nuclei were measured in the histologically normal appearing rectal mucosa. The between-case variability of nuclear abnormalities showed a very notable dispersion. A second order discriminant analysis showed a statistically significant correlation with recurrent disease; however, even cases labeled tentatively as "low risk" on the basis of their average nuclear abnormality had abnormality values suggesting a pre-neoplastic lesion. Cases with the highest nuclear abnormalities deviated as much as two standard deviations from normal. The nuclear abnormality distributions are shown in Fig. 11.

One can show a statistically significant difference between cases with recurrence and non-recurrent cases. The plot in Fig. 12 is based on the case mean discriminant function scores and nuclear abnormality values. It provides for a correct prediction of 49/57 cases for recurrence and of 45/72 for the non-recurrent cases.

3.4. Within-case heterogeneity

The assessment of chemopreventive efficacy is made more difficult by phenotypical heterogeneity of nuclei within a lesion. This applies to nuclei both from intraepithelial neoplastic (*i.e.*, premalignant) and pre-neoplastic lesions. An example is provided by nuclei recorded in tissue histopathologically labelled as endometrial atypical hyperplasia, from cases with co-occurring cancer and cases without an existing malignant endometrial lesion [42]. Unsupervised learning techniques [43,44] suggest that the nuclei sampled in these tissues belong to three different phenotypes. A progression curve was developed for the range of deviations from normal as one might find them from simple hyperplasia to adenocarcinoma. It provides some insight as to why such cases present such a diagnostic dilemma. All of the phenotypical subpopulations of the cases with co-existing adenocarcinoma are more progressed than the corresponding three subpopulations in cases free from malignant lesions. The most progressed subpopulation in the atypical hyperplasia cases with co-existing adenocarcinoma actually falls well into the range of abnormalities seen in adenocarcinoma lesions. The plot is shown in Fig. 13. The commonality of such phenotypical differences lends support to the practice of thresholding discussed earlier. Such an approach, by excluding more normal nuclear phenotypes, can in certain cases usefully focus analysis on the more progressed nuclei.

Phenotypical heterogeneity has been observed in pre-neoplastic lesions as well. Fig. 14 shows a progression curve for papillary lesions of the urothelium [45]. Nuclei measured in the histologically normal appearing tissue from cases harboring papillary carcinoma of grades 1–3 exhibit pre-neoplastic changes with slightly higher nuclear abnormalities than are observed in normal control nuclei. An unsupervised learning algorithm established that these nuclei contain two phenotypes, one with nuclear abnormalities very close to normal controls, and one with nuclear abnormalities in the range seen in grade 1 papillary carcinoma. This latter phenotype may contribute up to an average of 40% of nuclei in the histologically normal appearing tissue. Fig. 15 shows the nuclear signatures for the control nuclei, for the progressed phenotype from the pre-neoplastic lesion, and for nuclei from grade 1 papillary carcinoma.

3.5. Pre-neoplastic lesions/conditions in patients with or without premalignant or malignant lesions

Karyometric analyses have repeatedly demonstrated significant changes in histologically normal-appearing tissue from individuals who have co-occurring cancers or pre-cancerous lesions. This finding suggests potential utility of the method for better understanding progression and perhaps for early detection of lesions, both of which may be useful in the assessment of chemopreventive agents.

Previous karyometric work using breast tissue showed significant differences in histologic samples of normal appearing ductal epithelial cells from women with a remote breast cancer in the same breast as compared to samples from women with no cancer [6]. This work suggested that cells collected by ductal lavage or ductoscopy might similarly yield quantitative differences between nuclei from healthy breasts and those with existing disease. Breast ductal lavage samples were subsequently collected from 33 women across a range of four diagnostic categories defined as: (Normal) women with normal mammograms and considered at average risk for the development of breast cancer based on the Gail risk model [46]; women with normal mammograms, but considered at high risk based on the Gail

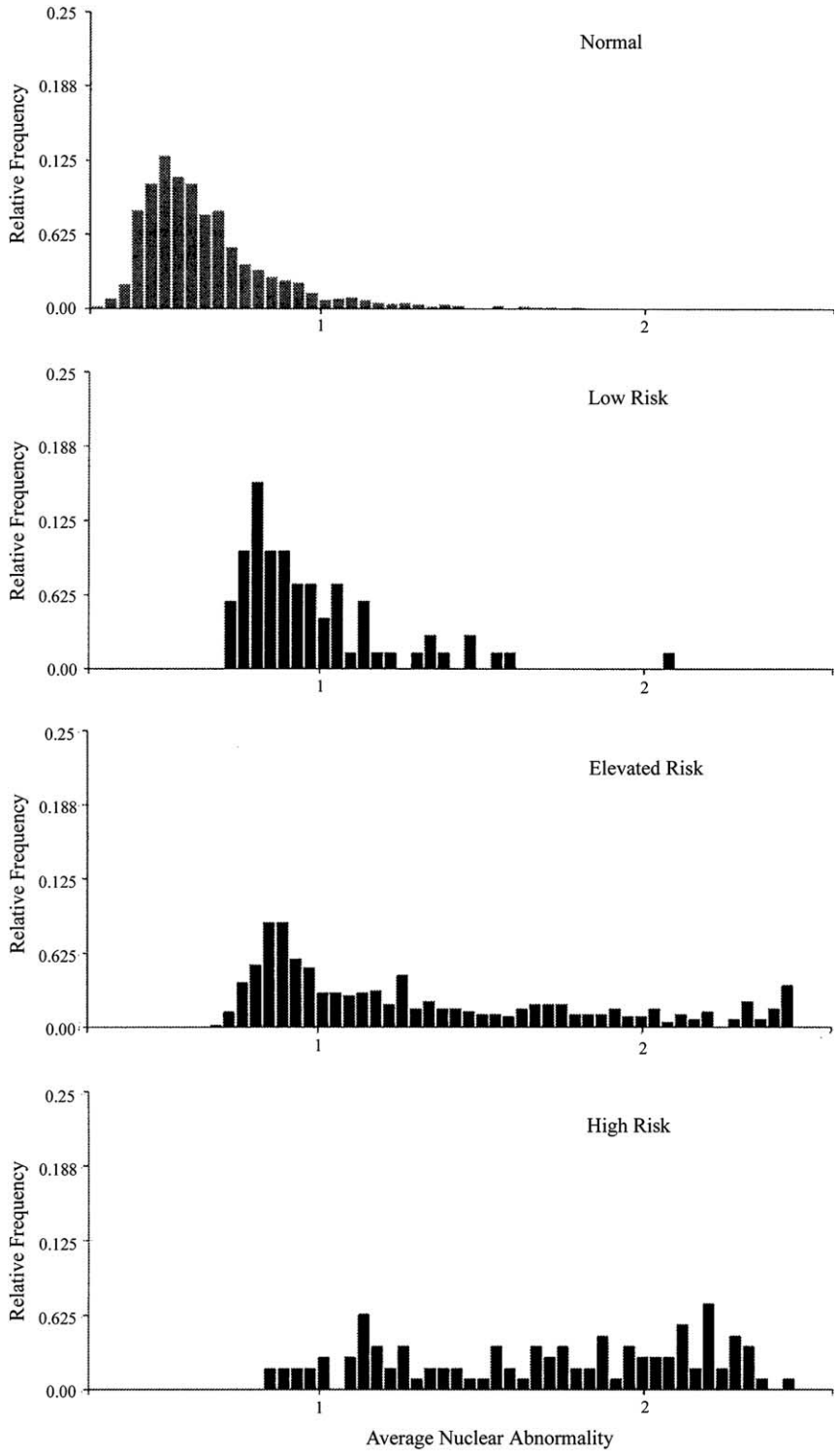

Fig. 11. Distributions of nuclear abnormality in histologically normal appearing rectal mucosa, from cases with a prior history of adenoma. Data derived from [20].

model, *i.e.*, a score of >1.7%; high risk (negative biopsy) women with an abnormal mammogram and a subsequent biopsy that was negative for cancer; and high risk (cancer) women with abnormal mammograms and a biopsy that was positive for carcinoma.

Fig. 16 shows the distribution of average nuclear abnormality for each group. Across the clinical diagnostic categories from normal to cases with a co-occurring cancer in the ipsilateral breast there is an increasing proportion of nuclei with nuclear abnormality scores greater

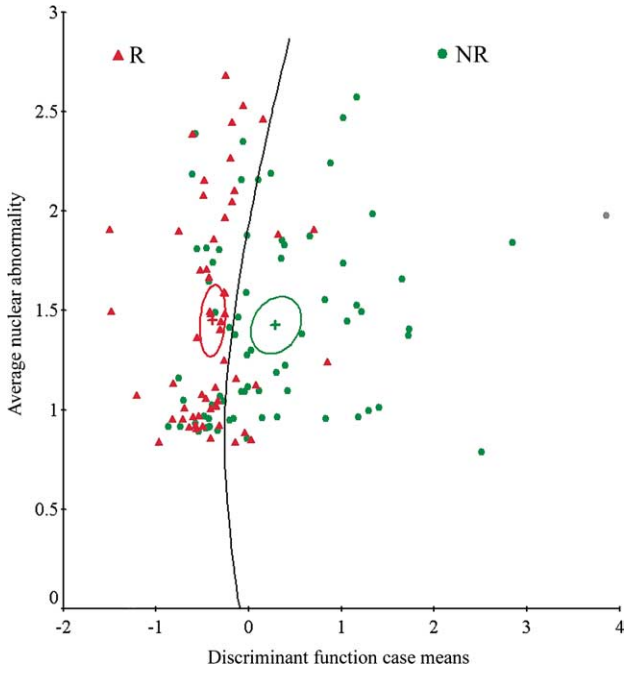

Fig. 12. Bivariate distribution of case averaged discriminant function values and nuclear abnormality for rectal mucosa samples from patients with a history of adenoma. R indicates recurrent and NR indicates non-recurrent cases. Shown are bivariate means, 95% confidence ellipses, and the Bayesian boundary between diagnostic categories. Data derived from [20].

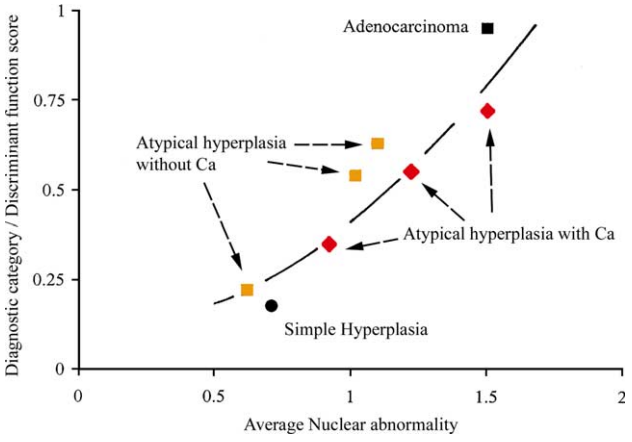

Fig. 13. Nuclear abnormality distributions in cells collected by ductal lavage from women with: a normal mammogram/low risk for breast cancer; a normal mammogram/high risk for breast cancer; an abnormal mammogram/negative biopsy; and an abnormal mammogram/positive biopsy. Data derived from [42].

than 1.0. This suggests that epithelial cell collection *via* minimally invasive procedures warrants further investigation for its ability to provide a clinically useful biomarker in the preneoplastic changes associated with risk of breast cancer.

Similar patterns have been detected in the case of ovarian tissue. Nuclei from histologically normal appearing epithelium of ovaries from patients free of

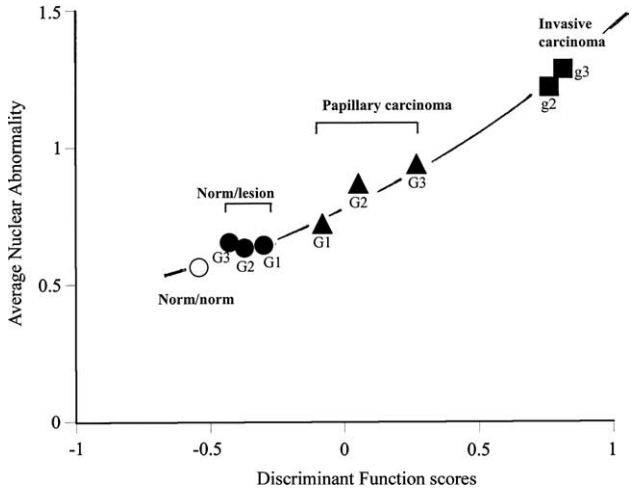

Fig. 14. Partial progression curve for endometrial lesions. Shown is the phenotypical heterogeneity of nuclei sampled from cases of atypical hyperplasia without and with co-occurring adenocarcinoma. Data derived from [45].

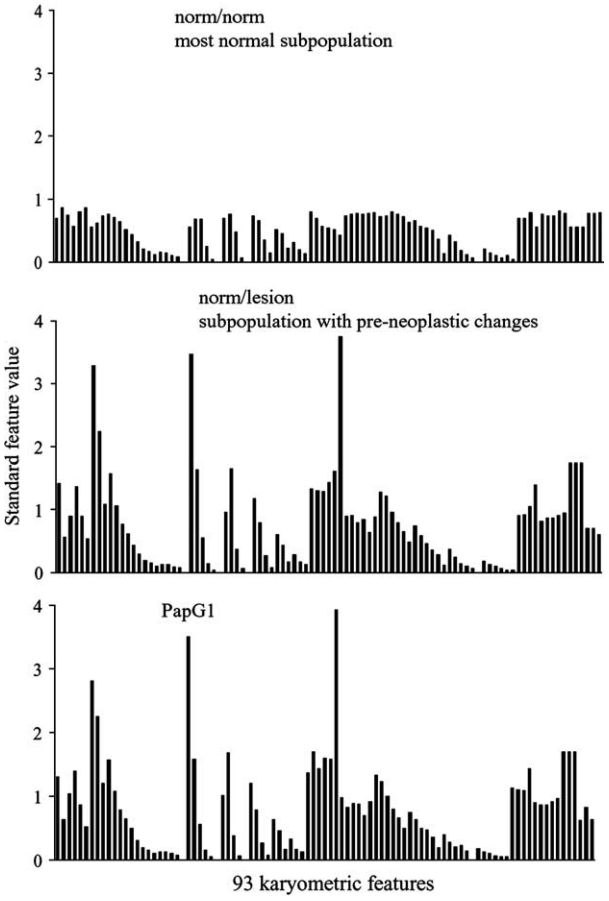

Fig. 15. Progression curve for papillary carcinoma of the urothelium. Note the pre-neoplastic lesion labeled "norm/lesion". Data derived from [45].

any ovarian lesion (norm/norm), from patients also free of any ovarian lesion but at high risk to develop ovarian cancer (norm/HR) and from cases with an existing

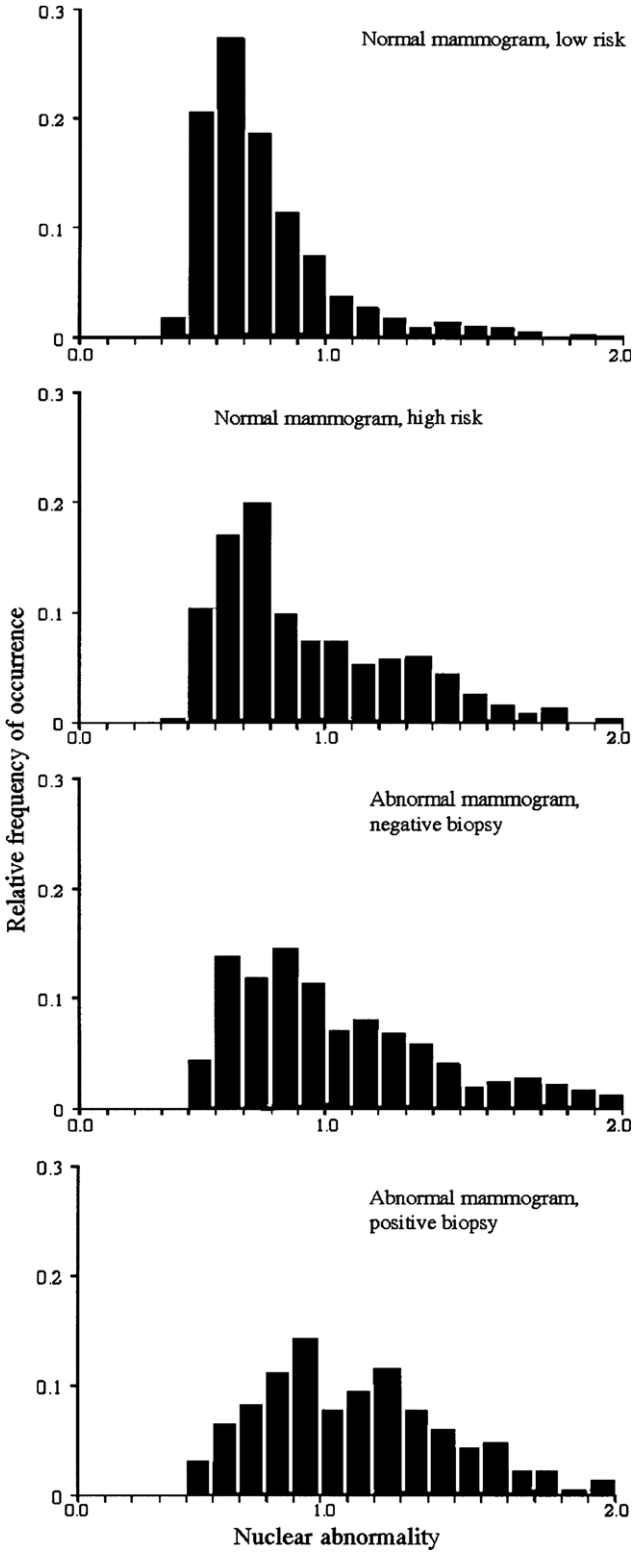

Fig. 16. Nuclear signatures from subpopulations in the pre-neoplastic urothelial lesions and of nuclei in grade 1 papillary carcinoma.

malignant ovarian lesion (norm/Ca) were recorded. A discriminant function was derived which, for the high-risk cases, shows a marked shift towards scores prevalent in the seemingly normal tissue from ovaries harboring a malignant lesion. This is seen in Fig. 17. In the samples recorded from the norm/norm and the norm/HR cases there was a large proportion of nuclei that were clearly normal. Drawing a threshold better separates out those nuclei showing pre-neoplastic change. Fig. 18 shows the bivariate mean values and corresponding 95% confidence ellipses for the nuclei falling onto the high value side of such a threshold. Two features were chosen for this display, a measure of dark pixels in the nucleus, and a measure of pixel optical density variance. The nuclei in these subsamples from the high-risk cases are very similar to those seen in ovaries harboring a malignant lesion, both seen in the upper right portion of the plot. They represent the pre-neoplastic change. Such changes were even seen in nuclei falling below the threshold, but recorded in cases that harbored an ovarian malignant lesion. The nuclei below threshold in norm/norm material and in norm/HR material are

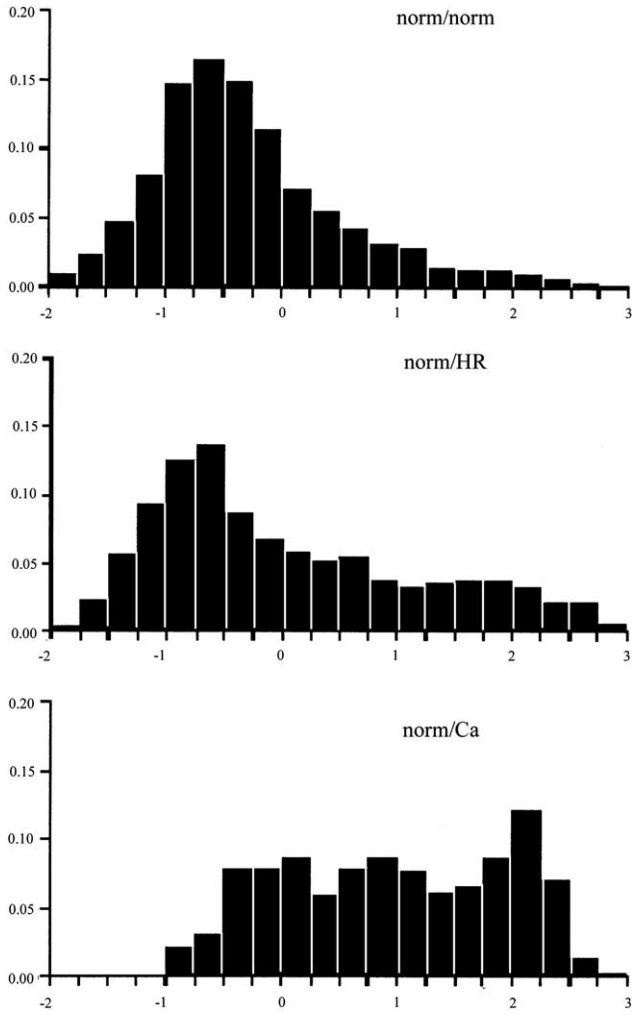

Fig. 17. Distribution of discriminant function scores for epithelial cells from normal epithelium of lesion-free ovaries, from normal-appearing epithelium of ovaries from women at high risk for ovarian cancer, and from the histologically normal-appearing epithelium of ovaries from women with ovarian cancer. Data derived from [8].

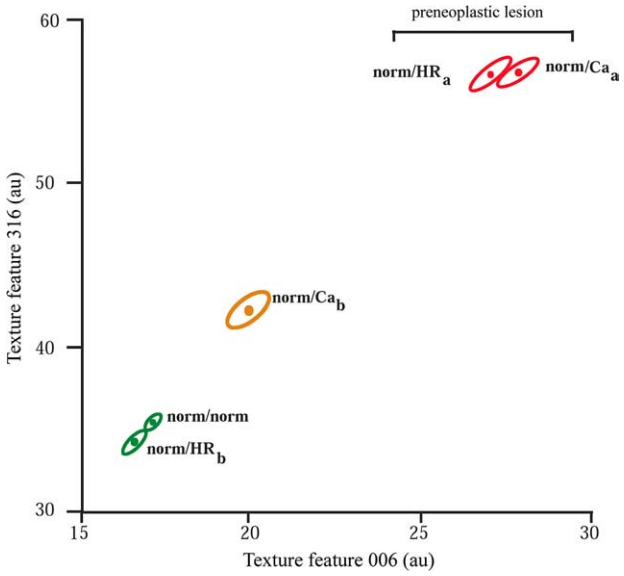

Fig. 18. Bivariate plot based on two nuclear chromatin texture features showing bivariate means and 95% confidence ellipses of nuclei from histologically normal appearing epithelium from patients at high risk for ovarian cancer or harboring an ovarian lesion. Data derived from [8].

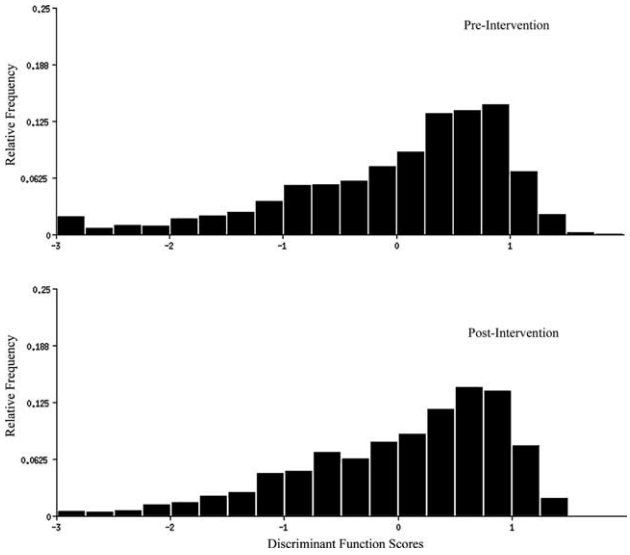

Fig. 19. Distribution of discriminant function scores for nuclei from sun-exposed skin before and after chemopreventive treatment for one year with 50000 IU daily of vitamin A. Data derived from [40].

very similar. The nuclei from the less progressed phenotype in cases of ovarian cancer occupy a central position.

3.6. Second order discriminant analysis

While previous examples have shown how average nuclear abnormality and discriminant function scores are useful in karyometric analyses, occasionally an even greater sensitivity of detection is called for. The determination of chemopreventive efficacy of orally given vitamin A (in the setting of a randomised, placebo-controlled chemoprevention trial), in cases of low-level solar actinic damage, provides an excellent example for the use of second order discriminant analysis to this end [39].

A first order discriminant function (DF I) had been developed to distinguish nuclei from skin biopsies taken at baseline from nuclei recorded in biopsies taken at end of study. The two discriminant function score distributions showed considerable overlap, due to substantial between-case variability. The overlap was in fact so severe that the 95% confidence intervals for the mean discriminant function scores also overlapped. The two distributions are shown in Fig. 19. At the distribution extremes, though, intervals could be found for which the relative frequencies of occurrence for the baseline and end of study observations differed significantly. One might now give up the large number of degrees of freedom offered by the sample size of nuclei – in this case $n = 5200$ – and rely on the within-case discriminant function score distributions, each based on 100 nuclei.

Now one has only the degrees of freedom offered by the number of cases, here 26 pairs of data sets. However, a discrimination now becomes possible in another feature space, based on the distributional properties of the within-case discriminant function scores. The relative frequencies of occurrence for each case, for selected intervals on the DF I score axis, are then used as "metafeatures" to derive a second order discriminant function (DF II). This approach allowed chemopreventive efficacy to be shown for 22/26 cases, or 85% of the post-intervention data. The distributions of the DF II scores are shown in Fig. 20.

A complete efficacy study might involve the recording of a dose–response curve. For the study of efficacy of orally given vitamin A such a curve is shown in Fig. 21. The abscissa is based on the proportion of cases with a second order discriminant function score reflecting a change in actinic damage. In the placebo group about 70% of cases had DF II scores indicating an increase in actinic damage. The 25, 50 and 75 K IU dose treatment groups all showed statistically significant changes towards diminished damage, with a dose response effect seen through the 50 K group. Although the reduced discriminant function scores were still in a range clearly deviating from normal, significant improvement occurred, and it is possible that a longer treatment period might have accomplished an even greater return to normalcy. As in the case of the DFMO study, this karyometric finding can be linked to a clinical outcome. In a previous study at the same institution, in which a similar design was used, 25000 IU vitamin A administered daily resulted in a statistically significant decline of 32% in incidence of squamous cell carcinoma [47].

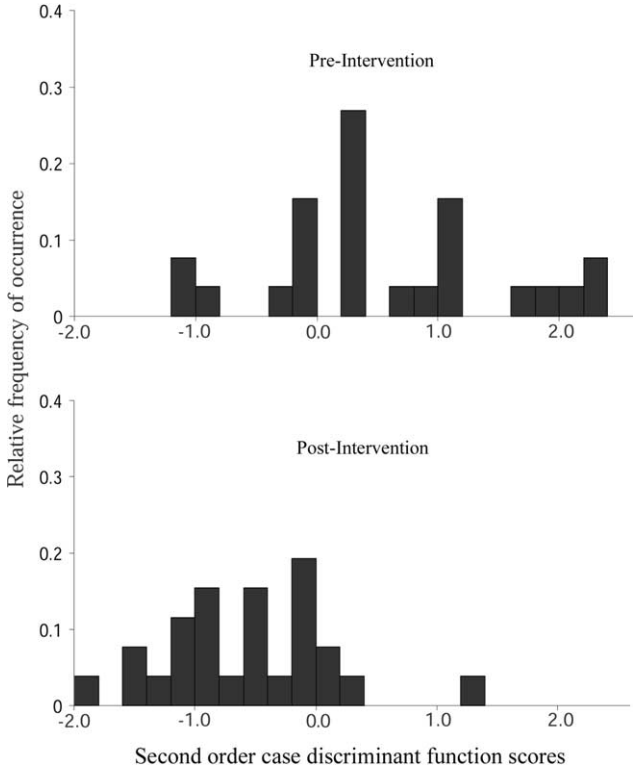

Fig. 20. Distribution of second-order discriminant function scores for the cases for which the distributions of nuclear discriminant function scores are shown in Fig. 19. Data derived from [40].

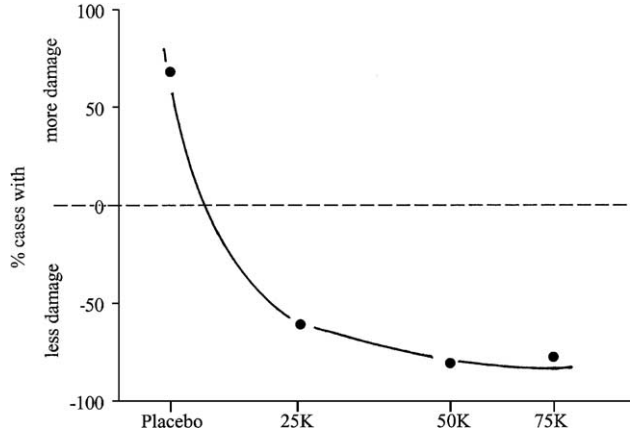

Fig. 21. Dose response to vitamin A treatment as represented by a measure based on discriminant function scores. Data derived from [40].

4. Discussion

The goals and methodologies suitable for studying the efficacy of a chemopreventive intervention are remarkably similar to those applied to the study of disease progression. A major advantage of a karyometric approach is the ability to measure progression of a pathologic process in a strictly quantitative fashion. There is no subjectivity involved in the extraction of karyometric features. The ability to subject the resulting information to rigorous statistical analysis is novel and represents a powerful methodological advance.

Nonetheless, the application of karyometry to chemoprevention is still a complicated task, due to the considerable heterogeneity existing among individuals, among tissue samples taken from individuals, and among nuclei within those samples. Essentially, the task of evaluating chemopreventive efficacy of a putative agent involves detecting changes in an environment with a low signal-to-noise ratio. Fortunately, extremely sensitive karyometric methods have been developed to address these issues. These methods render it feasible to exploit karyometric measurements as SEBMs, which act as integrating biomarkers, since karyometry examines the spatial patterns of the entire chromatin structure. In the case of nearly all cancers, progression is likely to occur through a variety of possible pathways, not all of which will share common intermediate steps. If SEBMs specific to a particular pathway are used, progression *via* other pathways may not be readily observable. Thus, the ability to detect chemopreventive effects will likewise be difficult. Karyometry, though, is likely to detect both progression and chemopreventive efforts to halt or reverse it, regardless of the pathways involved. The corresponding limitation is that when chemopreventive effects are observed via karyometric analysis, it is not possible to know which genetic and biochemical pathways are involved. However, a very economical strategy would entail the screening of chemopreventive agents using karyometry followed by investigation of specific mechanisms of action with pathway-targeted methods in the case of agents for which such knowledge is not already available.

Conflict of interest statement

None declared.

Acknowledgements

The research reported in this paper was supported in part by NIH/NCI Grants CA-41108 and CA-27502 to DSA, CA-82715 to FG, and CA-53877-09 to PHB.

References

1. Grundmann E, Stein P. Untersuchungen ueber die Kernstrukturen in normalen Geweben und im Carcinom. *Beitr Pathol Anat* 1968, **125**, 54–76.
2. Harbers E, Sandritter W. Gesteigerte Heterchromatisierung als pathogenetisches Prinzip. *Deutsche Med. Wochenschrift* 1968, **93**, 269–271.

3. Bartels PH, Montironi R, Hamilton PW, *et al*. Nuclear chromatin texture in prostatic lesions. II. PIN and malignancy associated changes. *Anal Quant Cytol Histol* 1998, **20**(5), 397–406.
4. Susnik B, Worth A, LeRiche J, *et al*. Malignancy associated changes in the breast. Changes in chromatin distribution in epithelial cells in normal appearing tissue adjacent to cancer. *Anal Quant Cytol Histol* 1995, **17**, 62–68.
5. King EB, Kromout LK, Chew KL, *et al*. Analytic studies of foam cells from breast cancer precursors. *Cytometry* 1984, **5**, 124–130.
6. Anderson NHJ, Kirk SJ, Frank D, *et al*. Malignancy-associated changes in lactiferous duct epithelium. *Anal Quant Cytol Histol* 2003, **25**(2), 63–72.
7. Brewer MA, Ranger-Moore J, Greene MH, *et al*. Preneoplastic changes in ovarian tissues. *Anal Quant Cytol Histol* 2004, **26**(4), 207–216.
8. Brewer MA, Ranger-Moore J, Baruche A, *et al*. Exploratory study of ovarian intraepithelial neoplasia. *Cancer Epidem Biomar Prevent* 2005, **14**(2), 299–305.
9. Wied GL, Bartels PH, Bibbo M, *et al*. Cytomorphometric markers for uterine cancer in intermediate cells. *Anal Quant Cytol Histol* 1980, **2**(4), 257–263.
10. Bibbo M, Bartels PH, Sychra JJ, *et al*. Chromatin appearance in intermediate cells from patients with uterine cancer. *Acta Cytol* 1981, **25**(1), 23–28.
11. Burger GJU, Rodenacker C. Changes in benign cell populations in cases of cervical cancer and its precursors. *Anal Quant Cytol Histol* 1981, **3**, 261–271.
12. Vooijs PG, Oud PS, Zahniser DJ, *et al*. Chromatin measurements in Feulgen stained intermediate cells from normal and abnormal cervical smears. *Analyt Quant Cytol* 1982, **4**, 154.
13. Reinhardt ER, Lenz R, Greiner W, *et al*. Diagnostic relevance of visually nonsuspect cells for cancer diagnosis. *Anal Quant Cytol Histol* 1982, **4**, 157.
14. Kwikkel HJ, Timmers T, Boone ME, *et al*. Relation of quantitative features of visually normal intermediate cells in cervical intraepithelial neoplasis I and II smears to progression or non-progression of the lesion. *Anal Quant Cytol Histol* 1987, **9**, 405–410.
15. Haroske G, Bernander ST, Koenig R, *et al*. Application of malignancy associated changes of the cervical epithelium in a hierarchic classification concept. *Anal Cell Path* 1990, **2**, 189–198.
16. Montag AG, Bartels PH, Lerma-Puertas E, *et al*. Karyometric marker features in tissue adjacent to *in situ* cervical carcinomas. *Anal Quant Cytol Histol* 1989, **11**(4), 275–280.
17. Bibbo M, Montag AG, Lerma-Puertas E, *et al*. Karyometric marker features in tissue adjacent to invasive cervical carcinomas. *Anal Quant Cytol Histol* 1989, **11**(4), 281–285.
18. MacAulay C, Lam S, Payner PW, *et al*. Malignancy associated changes in bronchial epithelial cells in biopsy specimens. *Anal Quant Cytol Histol* 1995, **17**, 55–71.
19. Montag AG, Bartels PH, Dytch HE, *et al*. Karyometric features in nuclei near colonic adenocarcinoma. Statistical analysis. *Anal Quant Cytol Histol* 1991, **13**(3), 159–167.
20. Ranger-Moore J, Frank D, Lance P, *et al*. Karyometry in rectal mucose of patients with previous colorectal adenomas. *Anal Quant Cytol Histol* 2005, **27**, 134–142.
21. daSilva VD, Prolla JC, Sharma P, *et al*. Karyometry in Barrett's Esophagus. *Anal Quant Cytol Histol* 2001, **23**(1), 40–46.
22. Bibbo M, Bartels PH, Galera-Davidson H, *et al*. Markers for malignancy in the nuclear texture of histologically normal tissue from patients with thyroid tumors. *Anal Quant Cytol Histol* 1986, **8**(2), 168–176.
23. Lerma-Puertas E, Galera-Davidson H, Bartels PH, *et al*. Karyometric marker features in fine needle aspirates of follicular adenoma of the thyroid. *Anal Quant Cytol Histol* 1990, **12**(4), 223–228.
24. Montironi R, Scarpelli M, Mazzucchelli R, *et al*. Subvisual chromatin changes are detected in the histologically normal urothelium in patients with synchronous papillary carcinoma. *Hum Pathol* 2003, **34**(9), 893–901.
25. Bartels PH, Montironi R, Hamilton PW, *et al*. Nuclear chromatin texture in prostatic lesions. I. PIN and adenocarcinoma. *Anal Quant Cytol Histol* 1998, **20**(5), 389–396.
26. Calaluce R, Kunkel M, Watts G, *et al*. Liminin-5-mediated gene expression in human prostate carcinoma cells. *Mol Carcinogen* 2001, **30**(2), 119–129.
27. Bartels PH, daSilva VD, Montironi R, *et al*. Chromatin texture signatures in nuclei from prostate lesions. *Anal Quant Cytol Histol* 1998, **20**(5), 407–416.
28. Bartels PH, Ranger-Moore J, Bartels HG, *et al*. Second order discriminant analysis in chemopreventive efficacy measurement. *Anal Quant Ctyol Histol* 2005, **27**, 15–26.
29. Tsybrovskyy O, Berghold A. Application of multilevel models to morphometric data. Part 1. Linear models and hypothesis testing. *Anal Cell Pathol* 2003, **25**, 173–185.
30. Tsybrovskyy O, Berghold A. Application of multilevel models to morphometric data. Part 2. Correlations. *Anal Cell Pathol* 2003, **25**, 187–191.
31. Ranger-Moore J, Bozzo P, Alberts DS, *et al*. Karyometry of nuclei from actinic keratosis and squamous cell cancer of the skin. *Anal Quant Ctyol Histol* 2003, **25**(6), 353–361.
32. Wolfe P, Murphy J, McGinley J, *et al*. Using nuclear morphometry to discriminate the tumorigenic potential of cells: a comparison of statistical methods. *Cancer Epidem Biomar Prevent* 2004, **13**(6), 976–988.
33. Raudenbush SW. Statistical analysis and optimal design in cluster randomized trials. *Psychol Meth* 1997, **2**(2), 173–185.
34. Garret JM. Sample size estimation for cluster designed samples. *Stat Tech Bull* 2001, **60**, 41–45.
35. Bartels PH, Garcia FAR, Davis J, *et al*. Progression curves for endometrial lesions. *Anal Quant Cytol Histol* 2001, **23**, 1–8.
36. Mariuzzi L, Mombello A, Rucco V, *et al*. Quantitative study of ductal breast cancer progression: signatures of nuclei in proliferating breast lesions and *in situ* cancers. *Adv Clin Path* 2000, **4**, 87–97.
37. Bartels PH, Thompson D, Montironi R, *et al*. Digital knowledge and diagnostic information. *J Histotechnol* 2000, **23**(3), 183–190.
38. Bozzo PD, Alberts DS, Vaught L, *et al*. Measurement of chemopreventive efficacy in skin biopsies. *Anal Quant Cytol Histol* 2001, **23**, 300–312.
39. Alberts DS, Ranger-Moore J, Einspahr J, *et al*. Safety and efficacy of dose-intensive oral vitamin A in subjects with sun-damaged skin. *Clin Cancer Res* 2004, **10**(6), 1875–1880.
40. Bartels PH, Ranger-Moore J, Stratton MS, *et al*. Statistical Analysis of chemopreventive efficacy of vitamin A in sun-exposed, normal skin. *Anal Quant Cytol Histol* 2002, **24**(4), 185–197.
41. Swed FS, Eisenhart C. Tables for testing randomness of grouping in a sequence of alternatives. *Annal Math Stat* 1943, **14**, 66–87., Table II.
42. Garcia F, Davis J, Alberts DS, *et al*. A karyometric approach to the characterization of atypical endometrial hyperplasia with and without co-ocurring adenocarcinoma. *Anal Quant Cytol Histol* 2003, **25**, 246–339.
43. McClellan RP. *Optimization and stochastic approximation techniques applied to unsupervised learning.* Master's thesis, Tucson: University of Arizona, 1971.
44. Bartels PH, Olson GB. Computer analysis of lymphocyte images. In Catsimpoolas N, ed. *Methods of cell separation*. New York, Plenum Press, 1980. pp. 1–99.
45. Montironi R, Scarpelli M, Mazzucchelli R, *et al*. Subvisual changes in chromatin organization state are detected by karyometry in the histologically normal urothelium in patients with synchronous papillary carcinoma. *Hum Pathol* 2003, **34**(9), 893–901.

46. Gail MH, Brinton LA, Byar DP, *et al*. Projecting individualized probabilities of developing breast cancer for white females who are being examined annually. *J Natl Cancer Inst* 1989, **81**(24), 1879–1886.

47. Moon TE, Levine N, Cartmel B, *et al*. Effect of retinol in preventing squamous cell skin cancer in moderate-risk subjects: a randomized, double-blind, controlled trial. *Cancer Epidem Biomar Prevent* 1997, **6**(11), 949–956.